Quadratic electroweak corrections for polarized Møller scattering

Aleksandrs Aleksejevs*
Memorial University, Corner Brook, Canada

Svetlana Barkanova†
Acadia University, Wolfville, Canada

Yury Kolomensky‡
University of California, Berkeley, USA

Eduard Kuraev§
Joint Institute for Nuclear Research, Dubna, Russia

Vladimir Zykunov¶
Belarussian State University of Transport, Gomel, Belarus

The paper discusses the two-loop (NNLO) electroweak radiative corrections to the parity violating $e^-e^- \to e^-e^-(\gamma)(\gamma\gamma)$ scattering asymmetry induced by squaring one-loop diagrams. The calculations are relevant for the ultra-precise 11 GeV MOLLER experiment planned at Jefferson Laboratory and experiments at future high-energy colliders. The imaginary parts of the amplitudes are taken into consideration consistently in both the infrared-finite and divergent terms. The size of the obtained partial correction is significant, which indicates a need for a complete study of the two-loop electroweak radiative corrections in order to meet the precision goals of future experiments.

I. INTRODUCTION

Polarized Møller scattering has been a well-studied low-energy reaction for close to eight decades now [1], but has attracted especially active interest from both experimental and theoretical communities due to the recent rapid progress in measuring spin-dependent observables. Since the nineties the interaction has allowed the high-precision determination of the electron-beam polarization at SLC [2], SLAC [3] [4], JLab [5] and MIT-Bates [6]. A Møller polarimeter may also be useful in future experiments planned at the ILC [7]. In addition, polarized Møller scattering can be an excellent tool for measuring parity-violating (PV) weak interaction asymmetries [8].

The first observation of Parity Violation in Møller scattering was made by the E-158 experiment at SLAC [9], which studied Møller scattering of 45- to 48-GeV polarized electrons on the unpolarized electrons in a hydrogen target. Its result at low $Q^2 = 0.026$ GeV^2, $A_{PV} = (1.31 \pm 0.14 \text{ (stat.)} \pm 0.10 \text{ (syst.)}) \times 10^{-7}$ [10] allowed one of the most important parameters in the Standard Model – the sine of the Weinberg angle – to be determined with an

---

*Electronic address: aaleksejevs@swgc.mun.ca
†Electronic address: svetlana.barkanova@acadiau.ca
‡Electronic address: yury@physics.berkeley.edu
§Electronic address: kuraev@theor.jinr.ru
¶Electronic address: vladimir.zykunov@cern.ch

accuracy of 0.5% ($\sin^2 \theta_W = 0.2403 \pm 0.0013$ in the $\overline{MS}$ scheme). A very promising experiment measuring the e-p scattering asymmetry currently running at Jefferson Lab, Qweak [11], aims to determine $\sin^2 \theta_W$ with relative precision of 0.3%. The next-generation experiment to study e-e scattering – MOLLER, planned at JLab following the 11 GeV upgrade – will offer a new level of sensitivity and measure the parity-violating asymmetry in the scattering of longitudinally polarized electrons off an unpolarized target to a precision of 0.73 ppb. That would allow a determination of the weak mixing angle with an uncertainty of ± 0.00026 (stat.) ± 0.00013 (syst.) [12], or about 0.1%, an improvement of a factor of five in fractional precision when compared with the E-158 measurement.

Since Møller scattering is a very clean process with a well-known initial energy and low backgrounds, any inconsistency with the Standard Model will signal new physics. Møller scattering experiments can provide indirect access to physics at multi-TeV scales and play an important complementary role to the LHC research program [13].

Obviously, before we can extract reliable information from the experimental data, it is necessary to take into account higher order effects of electroweak theory, i.e. electroweak radiative corrections (EWC). The inclusion of EWC is an indispensable part of any modern experiment, but will be of the paramount importance for the ultra-precise measurement of the weak mixing angle via 11 GeV Møller scattering planned at JLab. In general, from the theory point of view, the interpretability of e-e scattering is exceptionally good. However, to match the precision of MOLLER experiment, theoretical predictions for the PV e-e scattering asymmetry must include not only full treatment of one-loop radiative corrections (NLO) but also leading two-loop corrections (NNLO).

A significant theoretical effort has been dedicated to one-loop radiative corrections already. A short review of the literature to date on that topic is done in [14]. In [14], we also calculated a full gauge-invariant set of the one-loop EWC both numerically with no simplifications using FeynArts [15], FormCalc [16], LoopTools [16] and Form [17] as the base languages and by hand in a compact form analytically free from nonphysical parameters. The total correction was found to be close to -70%, and we found no significant theoretical uncertainty coming from the largest possible source, the hadronic contributions to the vacuum polarization. The dependence on other uncertain input parameters, like the mass of the Higgs boson, was below 0.1%.

It is possible that a much larger theoretical uncertainty in the prediction for the asymmetry may come from two-loop corrections. Paper [18] argued that the higher order corrections are suppressed by a factor of either about 0.1% or 5% (depending on a type of corrections) relative to the one-loop result. However, since the one-loop weak corrections for Møller scattering are so large and since the 11 GeV MOLLER experiment is striving for such unprecedented precision, we believe it is now worth looking into evaluating two-loop weak corrections.

One way to find some indication of the size of higher-order contributions is to compare results that are expressed in terms of quantities related to different renormalization schemes. In [19], we provided a tuned comparison between the result obtained with different renormalization conditions, first within one scheme then between two schemes. Our calculations in the on-shell and CDR schemes show a difference of about 11%, which is comparable with the difference of 10% between $\overline{MS}$ [20] and the on-shell scheme [18]. It is also worth noting that although two-loop corrections to the cross section may seem to be small, it is much harder to estimate their scale and behaviour for such a complicated observable as the parity-violating asymmetry to be measured by MOLLER experiment.
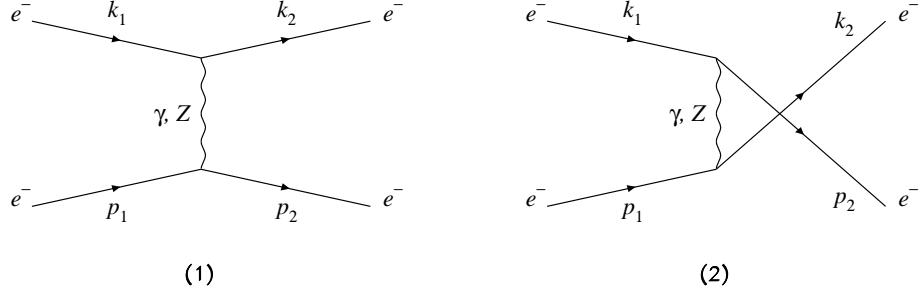
FIG. 1: *Diagrams describing nonradiative Møller scattering in the (1) t- and (2) u-channels.*

The two-loop EWC to the Born ($\sim M_0 M_0^+$) cross section can be divided into two classes: the Q-part induced by quadratic one-loop amplitudes ($\sim M_1 M_1^+$), and the T-part corresponding to the interference of the Born and two-loop diagrams ($\sim 2\mathrm{Re} M_0 M_{2-loop}^+$). The goal of this paper is to calculate the Q-part exactly. We show that the Q-part is much higher than the planned experimental uncertainty of MOLLER, which means that the two-loop EWC may be larger that previously thought. The large size of the Q-part demands a detailed and consistent consideration of the T-part, and that will be the next task of our group.

II. GENERAL NOTATIONS AND MATRIX ELEMENTS

Let us start by writing the cross section of polarized Møller scattering with the Born kinematics shown in Fig. 1,

$$e^-(k_1) + e^-(p_1) \rightarrow e^-(k_2) + e^-(p_2), \tag{1}$$

such that, with the appropriate accuracy for the present paper, we find:

$$\sigma = \frac{\pi^3}{2s}|M_0 + M_1|^2 = \frac{\pi^3}{2s}(M_0 M_0^+ + 2\mathrm{Re}M_1 M_0^+ + M_1 M_1^+). \tag{2}$$

Here, $\sigma \equiv d\sigma/d\cos\theta$, θ is the scattering angle of the detected electron with 4-momentum k_2 in the center-of-mass system of the initial electrons. The 4-momenta of initial (k_1 and p_1) and final (k_2 and p_2) electrons generate a standard set of Mandelstam variables:

$$s = (k_1 + p_1)^2, \ t = (k_1 - k_2)^2, \ u = (k_2 - p_1)^2. \tag{3}$$

It should also be noted that the electron mass m is disregarded wherever possible, in particular if $m^2 \ll s, -t, -u$.

M_0 and M_1 are the Born ($\mathcal{O}(\alpha)$) and one-loop ($\mathcal{O}(\alpha^2)$) amplitudes (matrix elements), respectively. Let us describe the structure of M_0:

$$M_0 = M_{0,t} - M_{0,u}, \ M_{0,u} = M_{0,t}(k_2 \leftrightarrow p_2), \ M_{0,t} = \sum_{j=\gamma,Z} M_t^j, \ M_t^j = i\frac{\alpha}{\pi}I_\mu^j D^{jt} J^{\mu,j}, \tag{4}$$

where the t-channel upper and lower electron leg currents are

$$I_\mu^j = \bar{u}(k_2)\gamma_\mu(v^j - a^j\gamma_5)u(k_1), \ \ J_\mu^j = \bar{u}(p_2)\gamma_\mu(v^j - a^j\gamma_5)u(p_1). \tag{5}$$

The squared Born amplitude M_0 forms the Born cross section:

$$\sigma_0 = \frac{\pi^3}{2s}M_0 M_0^+ = \frac{\pi\alpha^2}{s} \sum_{i,j=\gamma,Z} [\lambda_-^{i,j}(u^2 D^{it}D^{jt} + t^2 D^{iu}D^{ju}) + \lambda_+^{i,j}s^2(D^{it} + D^{iu})(D^{jt} + D^{ju})]. \tag{6}$$

A handy structure to use in the present study is

$$D^{ir} = \frac{1}{r - m_i^2} \ \ (i = \gamma, Z; \ r = t, u), \tag{7}$$

which depends on the Z-boson mass m_Z or on the photon mass $m_\gamma \equiv \lambda$. The photon mass is set to zero everywhere with the exception of specially-indicated cases where the photon mass is taken to be an infinitesimal parameter that regularizes the infrared divergence (IRD). Another set of useful functions is

$$\lambda_\pm^{i,k} = \lambda_{1B}^{i,k}\lambda_{1T}^{i,k} \pm \lambda_{2B}^{i,k}\lambda_{2T}^{i,k}, \tag{8}$$

These are combinations of coupling constants and $p_{B(T)}$, where $p_{B(T)}$ are the degrees of polarization of electrons with 4-momentum k_1 (p_1). More specifically,

$$\lambda_{1B(T)}^{i,j} = \lambda_V^{i,j} - p_{B(T)}\lambda_A^{i,j}, \ \lambda_{2B(T)}^{i,j} = \lambda_A^{i,j} - p_{B(T)}\lambda_V^{i,j},$$

$$\lambda_V^{i,j} = v^i v^j + a^i a^j, \ \lambda_A^{i,j} = v^i a^j + a^i v^j, \tag{9}$$

where

$$v^\gamma = 1, \ a^\gamma = 0, \ v^Z = (I_e^3 + 2s_W^2)/(2s_W c_W), \ a^Z = I_e^3/(2s_W c_W). \tag{10}$$

The subscripts L and R on the cross sections correspond to $p_{B(T)} = -1$ and $p_{B(T)} = +1$, where the first subscript indicates the degree of polarization for the 4-momentum k_1 and the second one indicates the degree of polarization for the 4-momentum p_1. Let us recall that $I_e^3 = -1/2$ and s_W (c_W) is the sine (cosine) of the Weinberg angle expressed in terms of the Z- and W-boson masses according to the rules of the Standard Model:

$$c_W = m_W/m_Z, \ s_W = \sqrt{1 - c_W^2}. \tag{11}$$

We can present the one-loop amplitude M_1 as a sum of boson self-energy (BSE), vertex (Ver) and box diagrams:

$$M_1 = M_{1,t} - M_{1,u}, \ M_{1,u} = M_{1,t}(k_2 \leftrightarrow p_2),$$
$$M_{1,t} = M_{\text{BSE},t} + M_{\text{Ver},t} + M_{\text{Box},t}. \tag{12}$$

We use the on-shell renormalization scheme from [21, 22], so there are no contributions from the electron self-energies. The question of the dependence of EWC on renormalization schemes and renormalization conditions (within the same scheme) was addressed in our earlier paper [19].
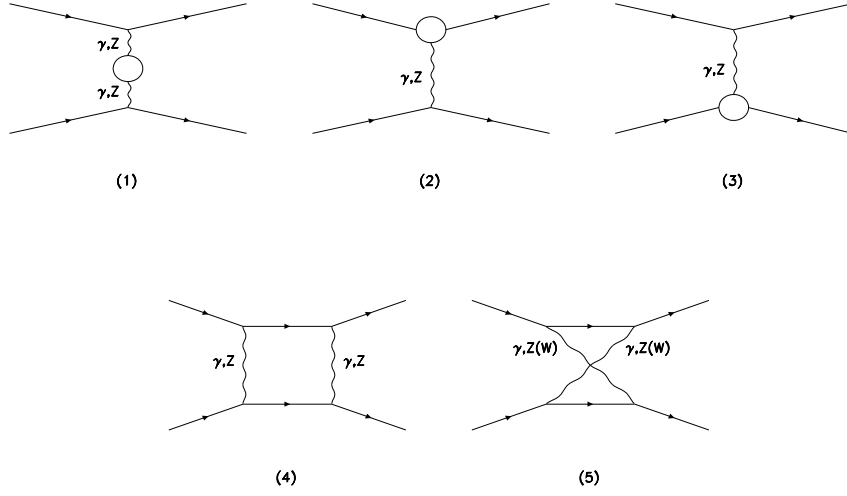
FIG. 2: *One-loop t-channel diagrams for the Møller process. The circles represent the contributions of self-energies and vertex functions. The u-channel diagrams are obtained via the interchange $k_2 \leftrightarrow p_2$.*

The infrared-finite BSE term can easily be expressed as:

$$M_{\text{BSE},t} = i\frac{\alpha}{\pi} \sum_{i,j=\gamma,Z} I_\mu^i D_S^{ijt} J^{\mu,j}, \tag{13}$$

with

$$D_S^{ijr} = -D^{ir} \hat{\Sigma}_T^{ij}(r) D^{jr}, \tag{14}$$

where $\hat{\Sigma}_T^{ij}(r)$ is the transverse part of the renormalized photon, Z-boson and γZ self-energies. The longitudinal parts of the boson self-energy make contributions that are proportional to m^2/r; therefore they are very small and are not considered here.

In order to get the electron vertex amplitude (2nd and 3rd diagrams in Fig. 2), we use the form factors $\delta F_{V,A}^{je}$ in the manner of paper [21], replacing the coupling constants v^j, a^j with form factors $v^{\gamma(Z)} \to \delta F_V^{\gamma(Z)e}$, $a^{\gamma(Z)} \to \delta F_A^{\gamma(Z)e}$. Then,

$$M_{\text{Ver},t} = \sum_{j=\gamma,Z} \left(M_{j/B,t} + M_{j/H,t} \right), \; M_{j/B,t} = i\frac{\alpha}{\pi} B_\mu^j D^{jt} J^{\mu,j}, \; M_{j/H,t} = i\frac{\alpha}{\pi} I_\mu^j D^{jt} H^{\mu,j}, \tag{15}$$

where the electron currents with vertices look like

$$B_\mu^j = I_\mu^j (v^j \to \delta F_V^{je}, \; a^j \to \delta F_A^{je}), \; H^{\mu,j} = J^{\mu,j} (v^j \to \delta F_V^{je}, \; a^j \to \delta F_A^{je}). \tag{16}$$

The infrared singularity is regularized by giving photon a small mass λ and in the t-channel vertex amplitude can be extracted in the form:

$$M_{\text{Ver},t}^\lambda = -\frac{\alpha}{\pi} \left(\log \frac{-t}{m^2} - 1 \right) \log \frac{s}{\lambda^2} M_{0,t}, \tag{17}$$

where e is the base of the natural logarithm. The rest (infrared-finite) part of t-channel vertex amplitude has the simple form The remaining (infrared-finite) part of the t-channel vertex

amplitude has a simple form convenient for analysis and coding:

$$M^f_{\text{Ver},t} = M_{\text{Ver},t} - M^\lambda_{\text{Ver},t} = M_{\text{Ver},t}(\lambda^2 \to s). \tag{18}$$

The box term can be presented as a sum of all two-boson contributions:

$$M_{\text{Box},t} = M_{\gamma\gamma,t} + M_{\gamma Z,t} + M_{Z\gamma,t} + M_{ZZ,t} + M_{WW,t}. \tag{19}$$

We need to account for both direct and crossed $\gamma\gamma$, γZ and ZZ-boxes:

$$M_{ij,t} = M^D_{ij,t} + M^C_{ij,t} \quad (i,j = \gamma, Z), \tag{20}$$

with $M^D_{ij,t}$ and $M^C_{ij,t}$ given by exact expressions in 4-dimensional integral form (4-point functions) by

$$
\begin{aligned}
M^D_{ij,t} = -i\left(\frac{\alpha}{\pi}\right)^2 \cdot \frac{i}{(2\pi)^2} \int & \frac{d^4k}{(k^2 - 2k_1 k)(k^2 + 2p_1 k)((q-k)^2 - m_j^2)(k^2 - m_i^2)} \times \\
& \times \bar{u}(k_2)\gamma^\mu(v^j - a^j\gamma_5)(\hat{k}_1 - \hat{k} + m)\gamma^\nu(v^i - a^i\gamma_5)u(k_1) \times \\
& \times \bar{u}(p_2)\gamma_\mu(v^j - a^j\gamma_5)(\hat{p}_1 + \hat{k} + m)\gamma_\nu(v^i - a^i\gamma_5 u(p_1),
\end{aligned}
\tag{21}
$$

$$
\begin{aligned}
M^C_{ij,t} = -i\left(\frac{\alpha}{\pi}\right)^2 \cdot \frac{i}{(2\pi)^2} \int & \frac{d^4k}{(k^2 - 2k_1 k)(k^2 - 2p_2 k)((q-k)^2 - m_j^2)(k^2 - m_i^2)} \times \\
& \times \bar{u}(k_2)\gamma^\mu(v^j - a^j\gamma_5)(\hat{k}_1 - \hat{k} + m)\gamma^\nu(v^i - a^i\gamma_5)u(k_1) \times \\
& \times \bar{u}(p_2)\gamma_\nu(v^i - a^i\gamma_5)(\hat{p}_2 - \hat{k} + m)\gamma_\mu(v^j - a^j\gamma_5)u(p_1).
\end{aligned}
\tag{22}
$$

Obviously, for WW-boxes we only need the crossed expression (22).

The infrared parts of the $\gamma\gamma$- and γZ-boxes in the t-channel are similarly given by

$$M^\lambda_{\gamma\gamma(\gamma Z + Z\gamma),t} = -\frac{\alpha}{\pi}\left(\frac{1}{2}\log\frac{-u}{s}\log\frac{-us}{\lambda^4} + \frac{\pi^2}{2} + i\pi\log\frac{s}{\lambda^2}\right)M_t^{\gamma(Z)}. \tag{23}$$

Using asymptotic methods, we can significantly simplify the box amplitudes containing at least one heavy boson (see, for example, [14], where simplifications were done on the cross-section level). Then

$$
\begin{aligned}
M^f_{\gamma Z,t} + M^f_{Z\gamma,t} = &\left(M_{\gamma Z,t} + M_{Z\gamma,t}\right) - \left(M^\lambda_{\gamma Z,t} + M^\lambda_{Z\gamma,t}\right) = -2i\left(\frac{\alpha}{\pi}\right)^2 \times \\
& \times \Bigg[\left(\frac{3}{2} + \log\frac{m_Z^2}{s}\right)\bar{u}(k_2)\gamma^\mu(v^Z - a^Z\gamma_5)(-\gamma^\alpha)\gamma^\nu u(k_1) \cdot \bar{u}(p_2)\gamma_\mu(v^Z - a^Z\gamma_5)\gamma_\alpha\gamma_\nu u(p_1) + \\
& + \left(\frac{3}{2} + \log\frac{m_Z^2}{-u}\right)\bar{u}(k_2)\gamma^\mu(v^Z - a^Z\gamma_5)\gamma^\alpha\gamma^\nu u(k_1) \cdot \bar{u}(p_2)\gamma_\nu\gamma_\alpha\gamma_\mu(v^Z - a^Z\gamma_5)u(p_1)\Bigg],
\end{aligned}
\tag{24}
$$

$$
\begin{aligned}
M_{ZZ,t} = -i\left(\frac{\alpha}{\pi}\right)^2 \frac{1}{16m_Z^2}\Bigg[& \bar{u}(k_2)\gamma^\mu(v^B - a^B\gamma_5)(-\gamma^\alpha)\gamma^\nu u(k_1) \cdot \bar{u}(p_2)\gamma_\mu(v^B - a^B\gamma_5)\gamma_\alpha\gamma_\nu u(p_1) + \\
& + \bar{u}(k_2)\gamma^\mu(v^B - a^B\gamma_5)\gamma^\alpha\gamma^\nu u(k_1) \cdot \bar{u}(p_2)\gamma_\nu\gamma_\alpha\gamma_\mu(v^B - a^B\gamma_5)u(p_1)\Bigg], \tag{25}
\end{aligned}
$$

$$M_{WW,t} = -i\left(\frac{\alpha}{\pi}\right)^2 \frac{1}{16m_W^2}\left[\bar{u}(k_2)\gamma^\mu(v^C - a^C\gamma_5)\gamma^\alpha\gamma^\nu u(k_1)\cdot\bar{u}(p_2)\gamma_\nu\gamma_\alpha\gamma_\mu(v^C - a^C\gamma_5)u(p_1)\right], \quad (26)$$

with the coupling-constants combinations for ZZ- and WW-boxes

$$v^B = (v^Z)^2 + (a^Z)^2, \ a^B = 2v^Za^Z, \ v^C = a^C = 1/(4s_W^2). \tag{27}$$

Now we are ready to present the one-loop complex amplitude as the sum of IR and IR-finite parts:

$$M_1 = M_1^\lambda + M_1^f, \ M_1^\lambda = \frac{\alpha}{\pi}\frac{1}{2}\delta_1^\lambda M_0, \ M_1^f = M_{\text{BSE}} + M_{\text{Ver}}^f + M_{\text{Box}}^f + M_a, \tag{28}$$

where

$$\delta_1^\lambda = 4B\log\frac{\lambda}{\sqrt{s}}, \tag{29}$$

and the complex value B can be presented in form (see, for example, [23])

$$B = \log\frac{tu}{m^2s} - 1 + i\pi. \tag{30}$$

The amplitudes from the non-factorized part of the boxes are given by

$$\text{Re}M_a = -\frac{\alpha}{2\pi}\left[(L_u^2 + \pi^2)M_{0,t} - (L_t^2 + \pi^2)M_{0,u}\right]. \tag{31}$$

where $L_r = \log(-s/r)$.

III. EXTRACTION OF INFRARED DIVERGENCES

Now we should make sure that the infrared divergences are cancelled. In a similar way as it was done for amplitudes, we present the complex interference term $\hat{\sigma}_1$ and differential cross section σ_Q as sums of λ-dependent (IRD-terms) and λ-independent (infrared-finite) parts:

$$\hat{\sigma}_1 = \frac{\pi^3}{s}M_1M_0^+ = \sigma_1^\lambda + \sigma_1^f, \quad \sigma_Q = \frac{\pi^3}{2s}M_1M_1^+ = \sigma_Q^\lambda + \sigma_Q^f. \tag{32}$$

The one-loop cross section which we denote $\sigma_1 = \text{Re}\hat{\sigma}_1$ was carefully evaluated with full control of the uncertainties in paper [14]. The term σ_Q (see (2)) is called the Q-part of the two-loop EWC and is the main subject of the present paper.

If we substitute the amplitudes derived in Section II to the left-hand-side of (2), and compare the result with the right-hand side of this equation, we will get the same expression for σ_1 as given in [14]. The simplest form for σ_1^λ (see formula (42) of [14]) is then:

$$\sigma_1^\lambda = \frac{\alpha}{\pi}\delta_1^\lambda\sigma_0. \tag{33}$$

The infrared-finite part σ_1^f can be conveniently to presented via the relative dimensionless correction:

$$\sigma_1^f = \frac{\alpha}{\pi}\delta_1^f\sigma_0. \tag{34}$$

After some transformations, the value σ_Q^λ is given by

$$\sigma_Q^\lambda = \frac{\pi^3}{2s} M_1^{\lambda+}\left(M_1^\lambda + 2M_1^f\right) = \frac{1}{4}\left(\frac{\alpha}{\pi}\right)^2 \mathrm{Re}\left[\delta_1^{\lambda*}(\delta_1^\lambda + 2\delta_1^f)\right]\sigma_0. \tag{35}$$

Finally, the infrared-finite part σ_Q^f expressed via the relative dimensionless corrections has form

$$\sigma_Q^f = \frac{\pi^3}{2s} M_1^f M_1^{f+} = \left(\frac{\alpha}{\pi}\right)^2 \delta_Q^f \, \sigma_0. \tag{36}$$

IV. BREMSSTRAHLUNG AND CANCELLATION OF INFRARED DIVERGENCES

To evaluate the cross section induced by the emission of one soft photon with energy less then ω, we follow the methods of [24] (see also [25]). Then this cross section can be expressed as:

$$\sigma^\gamma = \sigma_1^\gamma + \sigma_2^\gamma, \tag{37}$$

where $\sigma_{1,2}^\gamma$ have the similar factorized structure based on the factorization of soft-photon bremsstrahlung:

$$\sigma_1^\gamma = \frac{\alpha}{\pi}\mathrm{Re}\left[-\delta_1^\lambda + R_1\right]\sigma_0, \quad \sigma_2^\gamma = \frac{\alpha}{\pi}\mathrm{Re}\left[(-\delta_1^\lambda + R_1)^*\hat{\sigma}_1\right], \tag{38}$$

where

$$R_1 = -4B\log\frac{\sqrt{s}}{2\omega} - \log^2\frac{s}{em^2} + 1 - \frac{\pi^2}{3} + \log^2\frac{u}{t}. \tag{39}$$

The first part of the soft-photon cross section, σ_1^γ, cancels the IRD at the one-loop order, while the second part, σ_2^γ, cancels the IRD a the two-loop order, with half of σ_2^γ going to the cancellation of IRD in the Q-part and the other half going to treat IRD in the T-part:

$$\sigma_Q^\gamma = \sigma_T^\gamma = \frac{1}{2}\sigma_2^\gamma. \tag{40}$$

To obtain the term $-\delta_1^\lambda + R_1$ in Eq. (38), we must calculate the 3-dimensional integral over the phase space of one real soft photon. It can be done according to [24] in c.m.s:

$$-\delta_1^\lambda + R_1 = L(\lambda,\omega) = -\frac{1}{4\pi}\int\limits_{k_0<\omega}\frac{d^3k}{k_0}T^\beta(k)T_\beta(k), \tag{41}$$

where

$$T^\alpha(k) = \frac{k_1^\alpha}{k_1 k} - \frac{k_2^\alpha}{k_2 k} + \frac{p_1^\alpha}{p_1 k} - \frac{p_2^\alpha}{p_2 k}. \tag{42}$$

The difference between the estimation relying on the soft part only and the result obtained by separation into the soft and hard parts at lowest order is rather small (see [14]), so we believe that the soft cross section will provide the sufficient accuracy at second order as well.

At last, the cross section induced by the emission of two soft photons with a total energy less then ω can be written as:

$$\sigma^{\gamma\gamma} = \frac{1}{2}\left(\frac{\alpha}{\pi}\right)^2\left(\left|-\delta_1^\lambda + R_1\right|^2 - R_2\right)\sigma_0, \tag{43}$$

where $\frac{1}{2}$ is a statistical factor caused by the indistinguishability of two final photons and $R_2 = \frac{8}{3}\pi^2|B|^2$. The detailed calculations of $\sigma^{\gamma\gamma}$ are shown in Appendix A.

Just like σ^γ, the cross section $\sigma^{\gamma\gamma}$ is divided into equal halves, with a half going to cancel the IRD in the Q-part and a half going to the T-part:

$$\sigma_Q^{\gamma\gamma} = \sigma_T^{\gamma\gamma} = \frac{1}{2}\sigma^{\gamma\gamma}. \tag{44}$$

Combining all the terms together, we get the infrared-finite result at both the first and second orders. The first(second) order is given by the first(second) term on the LHS of the equation below:

$$\mathrm{Re}[\sigma_1+\sigma_1^\gamma]+(\sigma_Q+\sigma_Q^\gamma+\sigma_Q^{\gamma\gamma}) = \frac{\alpha}{\pi}\mathrm{Re}[R_1+\delta_1^f]\sigma_0 + \left(\frac{\alpha}{\pi}\right)^2\mathrm{Re}[\frac{1}{2}R_1^*\delta_1^f+\delta_Q^f+\frac{1}{4}R_1^*R_1-\frac{1}{4}R_2]\sigma_0. \tag{45}$$

V. NUMERICAL RESULTS

For the numerical calculations we use $\alpha = 1/137.035999$, $m_W = 80.398$ GeV, and $m_Z = 91.1876$ GeV as input parameters in accordance with [26]. The electron, muon, and τ-lepton masses are taken to be $m_e = 0.510998910$ MeV, $m_\mu = 0.105658367$ GeV, $m_\tau = 1.77684$ GeV, while the quark masses for vector boson self-energy loop contributions are taken to be $m_u = 0.06983$ GeV, $m_c = 1.2$ GeV, $m_t = 174$ GeV, $m_d = 0.06984$ GeV, $m_s = 0.15$ GeV, and $m_b = 4.6$ GeV. The values of the light quark masses were extracted using the fact that they provide shifts in the fine structure constant due to hadronic vacuum polarization $\Delta\alpha_{had}^{(5)}(m_Z^2)=0.02757$ [27], where

$$\Delta\alpha_{had}^{(5)}(s) = \frac{\alpha}{3\pi}\sum_{f=u,d,s}Q_f^2\left(\log\frac{s}{m_f^2}-\frac{5}{3}\right), \tag{46}$$

and Q_f is the electric charge of fermion f in proton charge units q $(q=\sqrt{4\pi\alpha})$.

On the other hand, the contribution of hadronic vacuum polarization to the fine structure constant also can be evaluated using the dispersion relation:

$$\Delta\alpha_{had}^{(5)}(s) = -\frac{s}{4\pi^2\alpha}\mathcal{P}\int_{2M_\pi^2}^{\infty}ds'\frac{\sigma_h(s')}{s'-s-i0}, \tag{47}$$

where $\mathcal{P}$ means that the principle value of the integral should be considered and $\sigma_h(s)$ is the cross section of hadron production in e^+e^- annihilation. In the case of small energies this cross section can be approximated by the cross section of the pion production channel $e^+e^-\to\pi^+\pi^-$:

$$\sigma_h(s) = \frac{\pi\alpha^2}{3s}\beta_\pi^3, \qquad \beta_\pi = \sqrt{1-\frac{4M_\pi^2}{s}}, \tag{48}$$

thus giving the following contribution to $\Delta\alpha_{had}^{(5)}(s)$:

$$\Delta\alpha_{had}^{(5)}(s) = \frac{\alpha}{\pi}\left(\frac{1}{12}\log\left(\frac{1+\beta_\pi}{1-\beta_\pi}\right)-\frac{2}{3}-2\beta_\pi^2\right). \tag{49}$$

Using Eq. (46) and Eq. (49) we can incorporate the use of the light quark masses as parameters regulated by the hadronic vacuum polarization in our calculations.
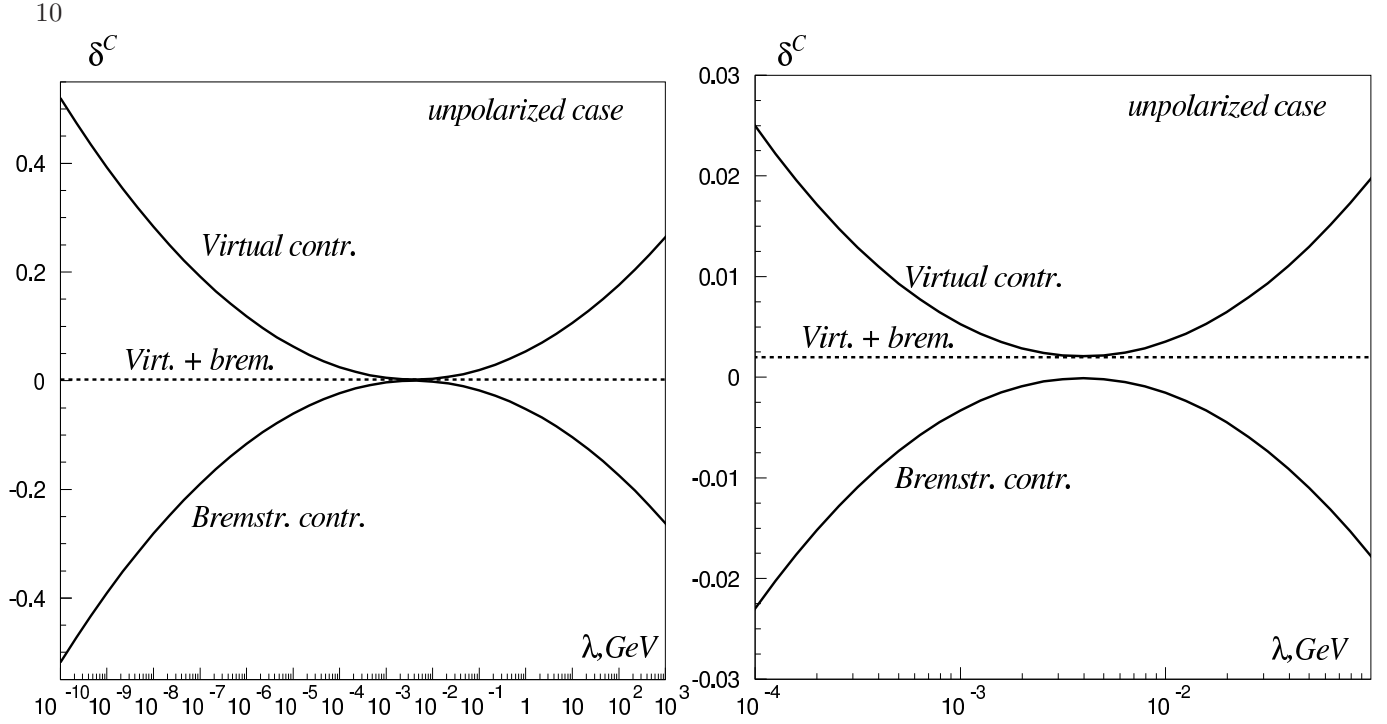
FIG. 3: *Virtual and bremstrahlung contributions to the relative correction to unpolarized cross section vs. the photon mass λ at $\theta = 90^o$ and $E_{\mathrm{lab}} = 11$ GeV.*

Finally, for the mass of the Higgs boson, we take $m_H = 115$ GeV. Although this mass is still to be determined experimentally, the dependence of EWC on m_H is rather weak. For the maximum soft photon energy we use $\omega = 0.05\sqrt{s}$, according to [14] and [28].

Let us define the relative corrections to the Born cross section due to a specific type of contributions (labeled by C) as

$$\delta^{\mathrm{C}} = (\sigma^{\mathrm{C}} - \sigma^0)/\sigma^0, \quad \mathrm{C} = 1\text{-loop}, \mathrm{Q}, \mathrm{T}, ...$$

The parity-violating asymmetry is defined in a traditional way,

$$A_{LR} = \frac{\sigma_{LL} + \sigma_{LR} - \sigma_{RL} - \sigma_{RR}}{\sigma_{LL} + \sigma_{LR} + \sigma_{RL} + \sigma_{RR}} = \frac{\sigma_{LL} - \sigma_{RR}}{\sigma_{LL} + 2\sigma_{LR} + \sigma_{RR}}, \qquad (50)$$

and the relative correction to the Born asymmetry due to C-contribution is defined as

$$\delta_A^{\mathrm{C}} = (A_{LR}^{\mathrm{C}} - A_{LR}^0)/A_{LR}^0.$$

Fig. 3, plotted for $\theta = 90^o$ and $E_{\mathrm{lab}} = 11$ GeV, clearly demonstrates that the relative correction to the unpolarized cross section is independent of the photon mass λ. We can also see a quadratic dependence on the log scale of λ for both the virtual and bremstrahlung contributions.

The left frame of Fig. 4 depicts the relative corrections to the asymmetry at $E_{\mathrm{lab}} = 11$ GeV versus the scattering angle θ in c.m.s. The lower line shows the corrections to the asymmetry with only one-loop EWC taken into account, and the upper line shows the combined one-loop and Q-part corrections. As expected, both of them are symmetric along the line $\theta = \pi/2$, have a minimum at $\theta = 90^o$, and depend on the scattering angle quite weakly.

The difference of these two effects is an absolute correction defined by

$$\Delta_A = (A_{LR}^{1-\mathrm{loop}+\mathrm{Q}} - A_{LR}^0)/A_{LR}^0 - (A_{LR}^{1-\mathrm{loop}} - A_{LR}^0)/A_{LR}^0 = (A_{LR}^{1-\mathrm{loop}+\mathrm{Q}} - A_{LR}^{1-\mathrm{loop}})/A_{LR}^0$$
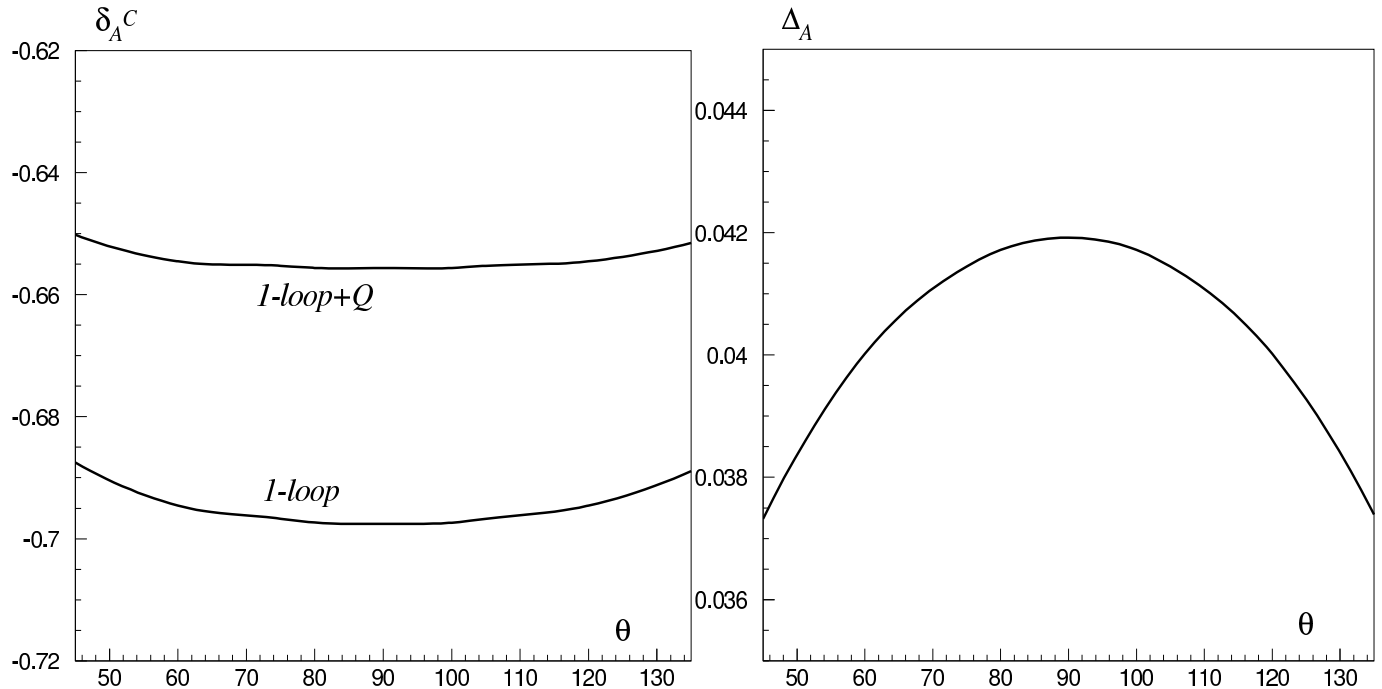
FIG. 4: *The relative corrections to the asymmetry (left) and the absolute correction Δ_A (right) vs scattering angle θ.*

and depicted in the right frame of Fig. 4. Here we can see that the Q-part gives quite a significant contribution, with Δ_A reaching a maximum of 0.0419 at $\theta = 90^o$. Taking into account that MOLLER's planned experimental error to the PV asymmetry is $\sim 2\%$ or less, we see that it is necessary to continue to work on the two-loop EWC, staring from the T-part.

Fig. 5 shows the relative (labeled as 1-loop and 1-loop+Q) corrections and absolute Δ_A corrections (labeled by Q) versus $\sqrt{s}$ at $\theta = 90^o$. In the high-energy region ($\sqrt{s} \geq 50$ GeV) our one-loop result (see [14]) is in excellent agreement with the result from [28] if we use the same set of Standard Model parameters. As one can see from Fig. 5, the scale of the Q-part contribution in the low-energy region is approximately constant, but grows sharply at $\sqrt{s} \geq m_Z$, where the weak contribution becomes comparable to the electromagnetic. This increasing importance of the two-loop contribution at higher energies may have a significant effect on the asymmetry measured at future e^-e^--colliders.

VI.   CONCLUSIONS

Experimental investigation of Møller scattering is not only one of the oldest tools of modern physics, but also a powerful probe of new physics effects. The new ultra-precise measurement of the weak mixing angle via 11 GeV Møller scattering planned at JLab (MOLLER) – as well as experiments proposed at future high-energy electron colliders – will require that the higher-order effects to be taken into account with the highest precision possible.

In this work, we build on the study of the one-loop electroweak radiative corrections to the cross-section asymmetry of the polarized Møller scattering at 11 GeV initiated by our group in [14], and address some of the two-loop effects. At this stage, we perform a detailed calculation for the part of the two-loop electroweak radiative correction induced by squaring one-loop diagrams.
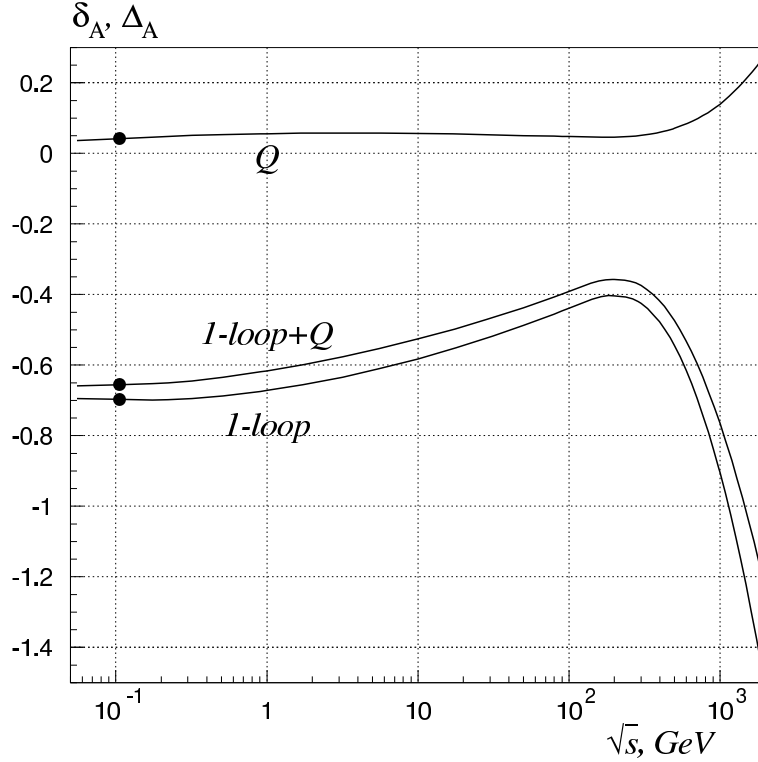
FIG. 5: *Relative (labeled by 1-loop+Q and 1-loop) and absolute (labeled by Q) corrections to PV-asymmetry vs $\sqrt{s}$. The filled circle corresponds to our predictions for the MOLLER experiment.*

The two-loop EWC to the Born ($\sim M_0 M_0^+$) cross section is divided into the T-part, which is the interference of Born and two-loop diagrams ($\sim 2\mathrm{Re}M_0 M_{2-loop}^+$), and the Q-part, induced by quadratic one-loop amplitudes ($\sim M_1 M_1^+$), which we evaluate here. The results are presented in both numerical and analytical form, with the infrared divergence explicitly cancelled. Also, we clearly demonstrate the important role of the imaginary part of amplitude, which is consistently taken into consideration both in the infrared-finite and divergent terms.

As one can see from our numerical data, at the MOLLER kinematic conditions, the part of the NNLO EWC we considered in this work can increase the asymmetry by up to $\sim 4\%$. The corrections depend quite significantly on the energy and scattering angles; at the high-energy region of $\sqrt{s} \sim 1000$ GeV achievable in the planned experimental program of the ILC, the estimated contribution of the quadratic EWC can reach $+14\%$; for 3 TeV at CLIC, it would be $+42\%$. We see that the large size of the Q-part demands detailed and consistent consideration of the T-part, which will be the next task of our group. It is impossible to say at this time if the Q-part will be partially enhanced or cancelled by other two-loop radiative corrections, although it seems probable that the two-loop EWC may be larger than previously thought. Although an argument can be made that the two-loop corrections are suppressed by a factor of $\alpha\pi$ relative to the one-loop corrections (see [18], for example), we are reluctant to conclude that they can be dismissed, especially in the light of 2% uncertainty to the asymmetry promised by MOLLER.

Since the problem of EWC for the Møller scattering asymmetry is rather involved, a tuned step-by-step comparison between different calculation approaches is essential. One of the im-

portant results of this work is the correctness of our calculations, which was controlled by a comparison of the results obtained from the equations derived by hand with the numerical data obtained by a semi-automatic approach based on FeynArts, FormCalc, LoopTools and Form. These base languages have already been successfully employed in similar projects ([14], [19]), so we are highly confident in their reliability.

In the future, we plan to address the remaining two-loop electroweak corrections which may be required by the promised experimental precision of the MOLLER experiment and experiments planned at ILC.

VII.   ACKNOWLEDGMENTS

[1] C. Møller, Ann. der Physik **14**, 531 (1932).

[2] M. Swartz *et al.*, Nucl. Instum. Meth. A. **363**, 526 (1995).

[3] P. Steiner *et al.*, Nucl. Instum. Meth. A. **419**, 105 (1998).

[4] H. Band *et al.*, Nucl. Instum. Meth. A. **400**, 24 (1997).

[5] M. Hauger *et al.*, Nucl. Instum. Meth. A. **462**, 382 (2001).

[6] J. Arrington *et al.*, Nucl. Instum. Meth. A. **311**, 39 (1992).

[7] G. Alexander and I. Cohen, Nucl. Instrum. Meth. A. **486**, 552 (2002) [hep-ex/0006007].

[8] E. Derman and W. J. Marciano, Ann. Phys. **121**, 147 (1979).

[9] K. S. Kumar *et al.*, Mod. Phys. Lett. A **10**, 2979 (1995); Eur. Phys. J. A **32**, 531 (2007); SLAC E158 Collab. P. L. Anthony *et al.*, Phys. Rev. Lett. **92**, 181602 (2004) [hep-ex/0312035].

[10] P. L. Anthony *et al.*, Phys. Rev. Lett. **95**, 081601 (2005).

[11] S. Page, JLab E02-020 report to PAC (Qweak-doc-703-v5), at http://www.jlab.org/qweak/ (2007)

[12] J. Benesch *et al.*, www.jlab.org/~armd/moller_proposal.pdf (2008)

[13] C. A. Heusch, Int. J. Mod. Phys A **15**, 2347 (2000); J. L. Feng, Int. J. Mod. Phys. A **15**, 2355 (2000).

[14] A. Aleksejevs *et al.*, Phys. Rev. D **82**, 093013 (2010).

[15] T. Hahn, (2000) [arXiv:hep-ph/0012260v2].

[16] T. Hahn, M. Perez-Victoria, Comput. Phys. Commun. **118**, 153 (1999).

[17] J. Vermaseren, (2000) [math-ph/0010025].

[18] F. J. Petriello, Phys.Rev. D **67** (2003) 033006, [hep-ph/0210259].

[19] A. Aleksejevs *et al.*, arXiv:1010.4185v3 [hep-ph].

[20] A. Czarnecki and W. J. Marciano, Phys. Rev. D 53, 1066 (1996) [hep-ph/9507420].

[21] M. Böhm, H. Spiesberger, W. Hollik, Fortschr. Phys. **34**, 687 (1986).

[22] A. Denner, Fortsch. Phys. **41**, 307 (1993).

[23] E. A. Kuraev and V. S. Fadin, Yad. Fiz. **41**, 733 (1985).

[24] G. 't Hooft and M. Veltman, Nucl. Phys. B. **153**, 365 (1979).

[25] E. A. Kuraev, N. R. Merenkov, and V. S. Fadin, Yad. Fiz. **45**, 782 (1987).

[26] C. Amsler *et al.*, Phys. Lett. B **667**, 1 (2008).

[27] F. Jegerlehner, J. Phys. G. **29** 101 (2003) [hep-ph/0104304].

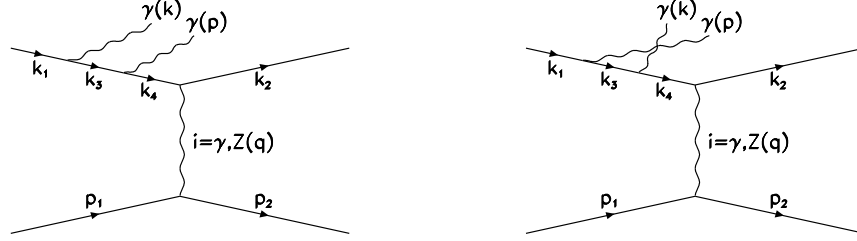[28] A. Denner and S. Pozzorini, Eur. Phys. J. C **7**, 185 (1999).

FIG. 6: *Double-bremsstrahlung diagrams for Møller scattering in t-channel corresponding to M_{11}^i. The u-channel diagrams are obtained by interchange $k_2 \leftrightarrow p_2$.*

Appendix A: Detailes of calculations for the case of emission of two real soft photons

First, let us calculate the amplitudes corresponding to the emission of two real soft photons (see Fig. 6),

$$e^-(k_1, \xi) + e^-(p_1, \eta) \to e^-(k_2) + e^-(p_2) + \gamma(k) + \gamma(p) \tag{A1}$$

in t- and u-channels with i-boson exchange ($i = \gamma, Z$). The amplitudes are labeled as M_{11}^i, M_{12}^i, M_{13}^i, ..., where the first (second) subscript denotes the origin of the first $\gamma(k)$ (second $\gamma(p)$) emitted photon: 1 – emitted from electron $e^-(k_1)$, 2 – from electron $e^-(k_2)$, 3 – from electron $e^-(p_1)$ and 4 – from electron $e^-(p_2)$. The exact expression for M_{11}^i is the following:

$$
\begin{aligned}
M_{11}^i = \quad & i(2\pi e)^4 N_{k_1} N_{k_2} N_{p_1} N_{p_2} N_p N_k \cdot \bar{u}(k_2)\gamma^\mu(v^i - a^i\gamma_5)\frac{1}{\hat{k}_4 - m}\gamma^\alpha e_\alpha(p)\frac{1}{\hat{k}_3 - m}\gamma^\beta e_\beta(k)u(k_1) \cdot \\
& \bar{v}(p_2)\gamma_\mu(v^i - a^i\gamma_5)v(p_1) \cdot \frac{1}{q^2 - m_i^2} \cdot \delta(k_1 + p_1 - k_2 - p_2 - k - p),
\end{aligned}
\tag{A2}
$$

where $N_k = \frac{1}{(2\pi)^{3/2}}\frac{1}{\sqrt{2k_0}}$. Using the Dirac equation and taking $k \to 0$, we can simplify

$$
\begin{aligned}
\frac{1}{\hat{k}_3 - m}\gamma^\beta u(k_1) \quad &= \frac{\hat{k}_1 - \hat{k} + m}{(k_1 - k)^2 - m^2}\gamma^\beta u(k_1) \approx \frac{\hat{k}_1 + m}{-2k_1 k}\gamma^\beta u(k_1) = \\
&= \frac{1}{-2k_1 k}(2k_1^\beta + \gamma^\beta[-\hat{k}_1 + m])u(k_1) = -\frac{k_1^\beta}{k_1 k}u(k_1).
\end{aligned}
\tag{A3}
$$

Analogously, at $k, p \to 0$,

$$\frac{1}{\hat{k}_4 - m}\gamma^\alpha u(k_1) = \frac{k_1^\alpha}{-k_1(k + p) + kp}u(k_1). \tag{A4}$$

Finally, the amplitude M_{11}^i at $k, p \to 0$ has the following form, with the convenient factorization from the Born amplitude:

$$M_{11}^i|_{k,p\to 0} = \quad e^2 N_p N_k \cdot e_\alpha(p)e_\beta(k) \cdot \frac{k_1^\alpha k_1^\beta}{(-k_1 k)(-k_1(k + p) + kp)} \cdot M_0^i. \tag{A5}$$

In the same manner, we get

$$M_{22}^i|_{k,p\to 0} = e^2 N_p N_k \cdot e_\alpha(p) e_\beta(k) \cdot \frac{k_2^\alpha k_2^\beta}{(k_2 p)(k_2(k+p) + kp)} \cdot M_0^i,$$

$$M_{12}^i|_{k,p\to 0} = e^2 N_p N_k \cdot e_\alpha(p) e_\beta(k) \cdot \frac{k_2^\alpha k_1^\beta}{(k_2 p)(-k_1 k)} \cdot M_0^i,$$

$$M_{33}^i|_{k,p\to 0} = e^2 N_p N_k \cdot e_\alpha(p) e_\beta(k) \cdot \frac{p_1^\alpha p_1^\beta}{(-p_1 k)(-p_1(k+p) + kp)} \cdot M_0^i,$$

$$M_{44}^i|_{k,p\to 0} = e^2 N_p N_k \cdot e_\alpha(p) e_\beta(k) \cdot \frac{p_2^\alpha p_2^\beta}{(p_2 p)(p_2(k+p) + kp)} \cdot M_0^i,$$

$$M_{34}^i|_{k,p\to 0} = e^2 N_p N_k \cdot e_\alpha(p) e_\beta(k) \cdot \frac{p_2^\alpha p_1^\beta}{(p_2 p)(-p_1 k)} \cdot M_0^i,$$

$$M_{13}^i|_{k,p\to 0} = e^2 N_p N_k \cdot e_\alpha(p) e_\beta(k) \cdot \frac{k_1^\alpha p_1^\beta}{(-k_1 p)(-p_1 k)} \cdot M_0^i,$$

$$M_{14}^i|_{k,p\to 0} = e^2 N_p N_k \cdot e_\alpha(p) e_\beta(k) \cdot \frac{k_1^\alpha p_2^\beta}{(-k_1 p)(p_2 k)} \cdot M_0^i,$$

$$M_{23}^i|_{k,p\to 0} = e^2 N_p N_k \cdot e_\alpha(p) e_\beta(k) \cdot \frac{k_2^\alpha p_1^\beta}{(k_2 p)(-p_1 k)} \cdot M_0^i,$$

$$M_{24}^i|_{k,p\to 0} = e^2 N_p N_k \cdot e_\alpha(p) e_\beta(k) \cdot \frac{k_2^\alpha p_2^\beta}{(k_2 p)(p_2 k)} \cdot M_0^i. \tag{A6}$$

Now we need to sum the terms generated by the substitution $k \leftrightarrow p$. For the 11–, 22–, 33–, 44–cases it works as the following:

$$M_{11}^i|_{k,p\to 0} + (k \leftrightarrow p) = e^2 N_p N_k M_0^i \Big(\frac{e_\alpha(p) e_\beta(k) k_1^\alpha k_1^\beta}{(-k_1 k)(-k_1(k+p) + kp)} + \frac{e_\alpha(k) e_\beta(p) k_1^\alpha k_1^\beta}{(-k_1 p)(-k_1(k+p) + kp)} \Big)$$

$$= e^2 N_p N_k M_0^i \Big(\frac{1}{-k_1 k} + \frac{1}{-k_1 p} \Big) \frac{e_\alpha(p) e_\beta(k) k_1^\alpha k_1^\beta}{(-k_1(k+p) + kp)}$$

$$\approx e^2 N_p N_k M_0^i \frac{e_\alpha(p) e_\beta(k) k_1^\alpha k_1^\beta}{(k_1 k)(k_1 p)}. \tag{A7}$$

As a result, the total $t(u)$-channel amplitude is given by

$$M_{t(u)}^i|_{k,p\to 0} = e^2 N_p N_k \cdot e_\alpha(p) e_\beta(k) \cdot T^\alpha(p) T^\beta(k) \cdot M_{0,t(u)}^i. \tag{A8}$$

Then, the cross section of (A1) has the form

$$\sigma^{\gamma\gamma} = \sigma_0 \frac{1}{2} \int\limits_{k_0+p_0<\omega} d^3k d^3p \cdot (eN_k)^2 (eN_p)^2 T^\alpha(p) T_\alpha(p) T^\beta(k) T_\beta(k)$$

$$= \sigma_0 \Big(\frac{\alpha}{\pi}\Big)^2 \frac{1}{2} \Big(\frac{1}{4\pi}\Big)^2 \int\limits_{k_0+p_0<\omega} \frac{d^3k}{k_0} \frac{d^3p}{p_0} \cdot T^\alpha(p) T_\alpha(p) T^\beta(k) T_\beta(k). \tag{A9}$$

It is possible to prove that

$$\left(\frac{1}{4\pi}\right)^2 \int\limits_{k_0+p_0<\omega} \frac{d^3k}{k_0}\frac{d^3p}{p_0} \cdot T^\alpha(p)T_\alpha(p)T^\beta(k)T_\beta(k) = |L(\lambda,\omega)|^2 - R_2. \qquad (A10)$$

If we change the condition $k_0 + p_0 < \omega$ to simply $k_0 < \omega$, $p_0 < \omega$, the term R_2 will go to zero. However, the conditions $k_0 < \omega$, $p_0 < \omega$ are not valid from the experiment point of view.

Let us calculate R_2 exactly. First, we introduce the notation

$$I(a_1, a_2; b_1, b_2) = \left(\frac{1}{4\pi}\right)^2 \int\limits_{a_1<k_0<a_2,\ b_1<p_0<b_2} \frac{d^3k}{k_0}\frac{d^3p}{p_0} \cdot T^\alpha(p)T_\alpha(p)T^\beta(k)T_\beta(k). \qquad (A11)$$

From Eq.(41) it is obvious that

$$I(0, a; 0, b) = L(\lambda, a)L(\lambda, b)^*, \qquad (A12)$$

which, of cause, works at $\lambda \ll a, b$ only. At $da, db \ll a, b$, the simple geometry considerations give the equation

$$I(a, a + da; b, b + db) = I(0, a + da; 0, b + db) + I(0, a; 0, b) - I(0, a; 0, b + db) - I(0, a + da; 0, b).$$

Simplifying using Eq.(A12) and Eq.(41), we get

$$I(a, a + da; b, b + db) = 16|B|^2 \log\frac{a + da}{a} \log\frac{b + db}{b} \approx 16|B|^2\frac{da}{a}\frac{db}{b}. \qquad (A13)$$

Finally, comparing Eq.(A10) and Eq.(A13), we conclude:

$$R_2 = \sum_\Omega I(a, a + da; b, b + db) = 16|B|^2 \int\limits_0^\omega \frac{da}{a} \int\limits_{\omega-a}^\omega \frac{db}{b} = 16|B|^2\text{Li}_2\left(\frac{a}{\omega}\right)\Big|_0^\omega = \frac{8}{3}\pi^2|B|^2. \quad (A14)$$

Here, $\Omega = \{a < \omega\} \cap \{b < \omega\} \cap \{a + b > \omega\}$. Our result for R_2 exactly agrees with [23].